MODELING OF REMOTE CONDENSING AMTEC CELLS

Joseph F. Ivanenok III and
Robert K. Sievers
Advanced Modular Power Systems
Ann Arbor, MI 48108
(313) 677-0516

William W. Schultz
Department of Mechanical Engineering and
Applied Mechanics
University of Michigan
Ann Arbor, MI 48109-2121
(313) 936-0351

Abstract

The Alkali Metal Thermal to Electric Converter (AMTEC) is a thermally regenerated sodium concentration cell that converts heat directly into electricity without moving parts. The high efficiency of AMTEC cells is useful for power generation in space and terrestrial applications (Ivanenok et al. 1993a, 1993b). One of the advanced features proposed in current high efficiency AMTEC cell designs is remote condensing. Remote condensing occurs when the condensing surface of the cell is thermally isolated from the high temperature β"-alumina solid electrolyte (BASE) tube. The parasitic heat losses are significantly reduced, thereby improving the cell efficiency. However, this configuration also increases the local Na vapor pressure (sodium concentration) on the cathode side of the BASE tube, and thus lowers the BASE tube's power output. The balance of these opposing effects is very important in optimizing system designs. This paper derives the equations necessary to calculate the vapor flow pressure drop, and compares the calculations to experimental data.

INTRODUCTION

The basic principles of AMTEC operation have been fully described (Weber 1974 and Hunt et al. 1975) and experiments have verified the basis for a general performance analysis (Williams et al. 1990 and Sievers et al. 1992). Current models predict that the decrease in parasitic heat loss (gain in efficiency) due to remote condensing is substantially greater than the loss of power density for typical cell designs. As cell efficiencies improve, the modeling must also improve to account for secondary effects that are negligible at lower efficiencies. Experiments were performed with a highly instrumented AMTEC cell to determine the effect of remote condensing (Sievers et al. 1993). This paper examines the data gathered during this experiment and shows the derivation and validation of pressure drop models developed to account for continuum, slip, and free molecular flow regimes.

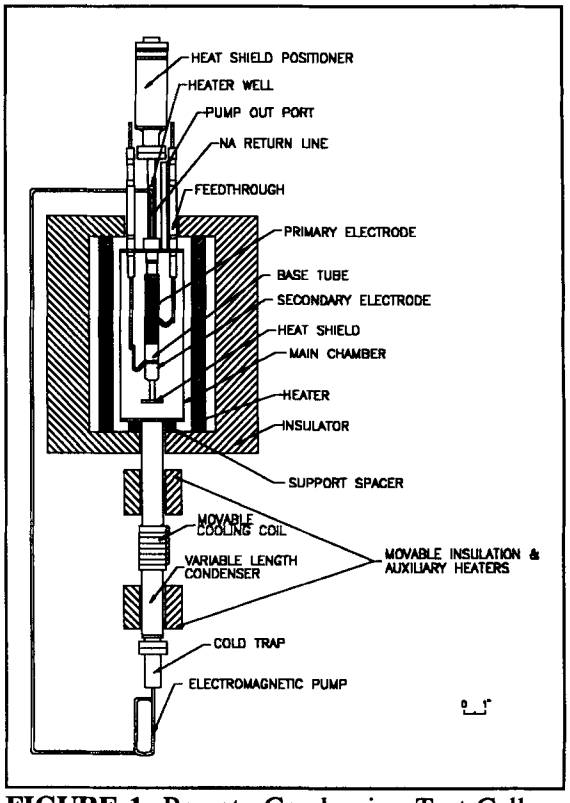

FIGURE 1. Remote Condensing Test Cell.

Test Cell Design

The test cell, and experimental data, have been discussed in detail by Sievers et al. (1993). However,

a brief description is included here as a basis for the modeling process. The remote condensing test cell, shown in Figure 1, has a large 7.5 cm diameter hot zone fully enclosing the BASE tube. This insures remote condensing by eliminating sodium condensation in the BASE tube/hot zone area. A heater on the outside of the cell maintains the temperature required to keep the sodium from condensing, and simulates the insulation package of a full space power system. A cartridge heater inside the BASE tube supplies the heat to run the AMTEC cell, and simulates the GPHS in a radioisotope powered system. Feedthroughs extend from the hot zone into cooler regions above the insulation.

The BASE tube is filled with liquid sodium and has two TiN electrodes on the outside; the primary power/sodium flow producing electrode, and a secondary electrode to "sense" the sodium vapor pressure in the hot zone. A voltage probe inside the BASE tube measures the potential in the sodium pool at the location of the secondary electrode, and a thermocouple (TC) well inside the BASE tube is used to measure the secondary electrode temperature. The sodium vapor pressure on the outside is determined from:

$$P_{vapor} = P_{sat} e^{-\frac{FV_{oc}}{RT_s}} \qquad (1)$$

where T_s is the temperature of the secondary electrode, P_{sat} is the saturated vapor pressure at the secondary electrode temperature, R is the universal gas constant, F is the Faraday constant, V_{oc} is the secondary electrode voltage at open circuit, and P_{vapor} is the sodium vapor pressure in the main chamber near the secondary electrode. This simple, well documented equation is used in all AMTEC models. A 2.5 cm diameter, approximately 25 cm long tube provides a variable length condenser. Both the axial location of the cooling coils and the condenser wall temperature can be varied. The vapor flow path length, and pressures, can therefore be varied to characterize remote condensing. A moveable heat shield plate can vary the vapor flow pressure drop. TC wells have been placed along the length of several components to monitor all cell temperature distributions and provide information for the thermal characteristics of AMTEC cells.

Pressure Drop Derivations

Typical AMTEC cells operate in three flow regimes, continuum, slip, and free molecular. Dushman (1962) categorized the flow of gases into the following three regions defined by the flow's dimensionless parameter the Knudsen (Kn) number:

Continuum (viscous)	$Kn \leq 0.01$
Slip (transition)	$0.01 \leq Kn \leq 1$
Free Molecular (molecular)	$1 \leq Kn$

There is an efficiency trade-off between the thermal resistance offered by the heat shields and their associated, power depleting, pressure drop. As AMTEC cells become more efficient the power loss due to the pressure drop becomes more important, and an accurate model of the pressure drop must treat all three flow regimes. The models developed, and used, up to this point consistently overpredict the pressure drop, but in the future may limit certain designs with this conservativism. The flow is assumed to be axisymmetric, steady, and isothermal (Partial derivatives are denoted by subscripts in this section, for example $\partial^2 w/\partial z^2 = w_{zz}$). We assume that the pressure and the density are functions only of the z-coordinate $\{P=P(z)$ and $\rho=\rho(z)\}$. These assumptions reduce the continunity equation to $(\rho w)_z = 0$ (where w is the velocity component in the z-direction, and ρ is the fluid density). The friction factor, which is a function of Reynolds (Re) number and the coefficient of slip (ζ), has no z dependence (ζ obviously represents a distance that can be described as that location on the other side of the wall where the velocity would go to zero for fully developed flow with no slip). The axial (z) component of the Navier-Stokes

equations reduces to the following:

$$P_z = \mu\left[w_{rr}+\frac{w_r}{r}+\frac{4}{3}w_{zz}\right]-\rho w w_{zz} \tag{2}$$

The velocity profile for the quasi-fully-developed ($\partial/\partial t \ll \partial/\partial r$) flow becomes $w(r,z)=A(z)+B(z)r^2$. Inserting w(r,z) into equation (2), and taking the required partial derivatives yields:

$$P_z = 4\mu B+\frac{4}{3}\mu(A_{zz}+B_{zz}r^2)-\rho(A+Br^2)(A_z+B_z r^2) \tag{3}$$

Applying the slip boundary condition ($w+\zeta w_r = 0$ at r=a where a is the radius of the flow channel) a relationship between A an B can be determined ($A = -Ba^2-2\zeta Ba$). With some integration and algebraic manipulation the friction factor (f) can be determined as a function of Re and ζ:

$$f=\frac{16}{Re\left[1+4\frac{\zeta}{a}\right]} \tag{4}$$

Kennard (1938) offers the following relationship between ζ and the mean free path (λ):

$$\zeta = 2c\frac{2-\eta}{\eta}\lambda \tag{5}$$

Where c is a number between 0.491 and 0.499, and η is the momentum transfer ratio (when $\eta=1$ the molecules are diffusely scattered, when $\eta=0$ specular reflection). Inserting equation (5) into equation (4) produces a useful equation for determining the friction factor:

$$f = \frac{16}{Re\left[1+8Kn\left(\frac{2-\eta}{\eta}\right)c\right]} \tag{6}$$

Taking the compressible flow pressure drop equation from Bird et al. (1960), adding a kinetic energy factor (α) from White (1986), and substituting the friction factor from Equation (6) the final compressibleflow pressure drop equation that is valid for continuum, and slip flow ($Kn \leq 1$) is as follows:

$$\alpha \ln\left[\frac{P_2}{P_1}\right] = \frac{1}{2}\left[\left(\frac{P_2}{P_1}\right)^2-1\right]\frac{RT_1}{MV_1^2}+\left[\frac{64l}{Re\left[1+8Kn\left(\frac{2-\eta}{\eta}\right)rc\right]}\right] \tag{7}$$

where P_1 is the pressure upstream and P_2 is the pressure downstream, T_1 is the average fluid temperature, V_1 is the average fluid velocity, M is the molecular weight of sodium, l is the tube length and r is the tube

radius. The value of α can be written as:

$$\alpha = \frac{\left[2+16Kn\left(\frac{2-\eta}{\eta}\right)c+64Kn^2\left(\frac{2-\eta}{\eta}\right)^2c^2\right]}{\left[8Kn\left(\frac{2-\eta}{\eta}\right)C+1\right]^2} \tag{8}$$

Kennard (1938) supplies the final required equation for the free molecular flow (modified with the momentum transfer ratio) through short tubes:

$$\Delta P = \frac{20+19\left(\frac{l}{r}\right)+3\left(\frac{l}{r}\right)^2}{20+8\left(\frac{l}{r}\right)} \frac{m}{r^2\sqrt{\frac{\pi M}{2RT}}\left(\frac{2-\eta}{\eta}\right)} \tag{9}$$

All of the equations from above are used to predict the pressure drop from the secondary electrode to the condenser. The test cell, Figure 1, was broken into the following three sections to simplify the pressure drop calculations: a) the annulus between the BASE tube and cell wall up to the heat shield; b) the heat shield c)the condenser tube. Kn numbers in each section are used both to determine which equations apply, and in the pressure drop calculation (an iterative solution is required). The molecular flow typically occurs in the condenser where the gas becomes rarefied. A linear merging function joins the continuum/slip flow with the molecular flow. Now that the equations have been developed and their use described their predictions can be compared to experimental data.

RESULTS

The model predictions were compared to the pressure drop determined experimentally, and found to agree well with the measured pressure drop in most flow regimes, especially in the (0 - 10 A) range in which the cells are expected to operate. At low flow rates the comparison is very good. At higher flow rates the predicted pressure drop is generally less than that measured. An assessment of the deviation at high flow rates suggests that the actual temperature of the secondary electrode was less than the measured temperature of the sodium inside the BASE tube at the same axial location. Sievers et al. (1993) describes the pressure drop deviation at high Na flow rates.

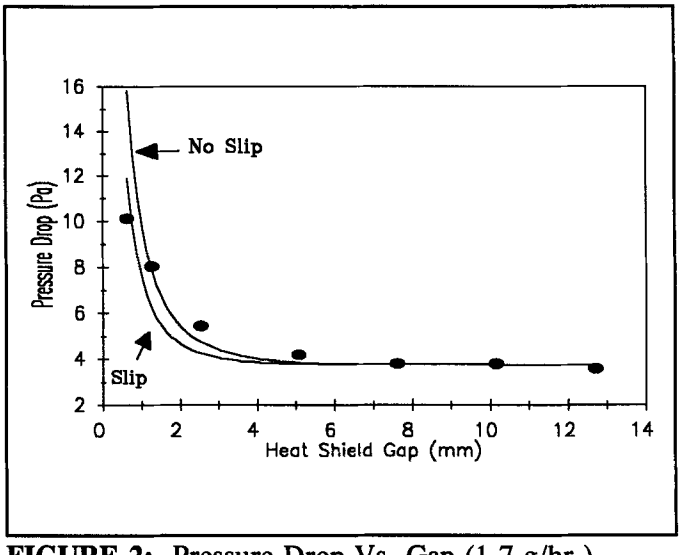

FIGURE 2: Pressure Drop Vs. Gap (1.7 g/hr.).

The effects of the heat shield flow gap on the pressure drop are shown, for moderate and prototypic flow rates, in Figures 2 and 3. These pressure drops were measured at two different flow rates. The flow rate in Figure 3 is typical of expected operating conditions. The circles represent the experimental data

while both the previous model and updated model predictions are included for completeness. Both compare well with the test data. Figure 2 shows that at low Na flow rate the slip model converges to the no slip model. Figure 3 demonstrates that the pressure drops at the higher Na flow rates are increasingly affected by slip forces. The remaining concern is the discrepancy between the model and the data at moderate heat shield gaps. The heat shield flows are modeled as sudden contractions and/or expansions, and this appears to be correct as the gap approaches either extreme. Investigation into this phenomena continues.

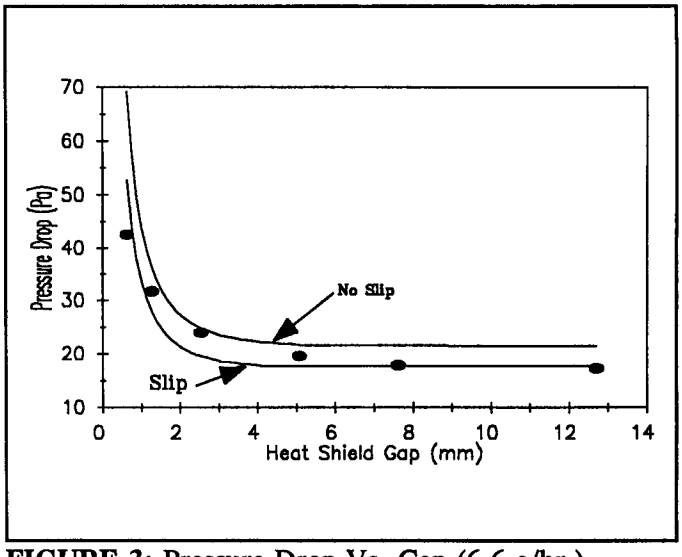

FIGURE 3: Pressure Drop Vs. Gap (6.6 g/hr.).

CONCLUSIONS

The model fits the data very well in the expected operating regime, and at low flow rates is identical (as expected) to the no slip pressure drop model, but appears to underpredict the pressure drop for very small heat shield gaps, and high Na flow rates. However, cells are not expected to operate in this regime. We believe the model is essentially correct and that the apparent discrepancy arises from the difficulties measuring the secondary electrode temperature at high Na flow rates, and the resulting over-estimate of the pressure in the electrode region. The model presented here is a useful tool in designing and analyzing the next, more efficient, generation of AMTEC cells.

Acknowledgments

The authors wish to thank the Air Force Phillips Laboratory for sponsoring the remote condensing tests, and its continued support of AMTEC technology. We would also like to thank D.A. Butkiewicz and J.E. Pantolin for their efforts in designing, fabricating, and operating the remote condensing test cell.

References

Bird, R.B., W.E. Stewart, and E.N. Lightfoot (1960), *Transport Phenomena*, John Wiley & Sons: New York.

Dushman, Saul (1962), *Scientific Foundations of Vacuum Technique,* Second Edition; John Wiley & Sons: New York.

Hunt, T.K., N. Weber, and T. Cole (1975), "Output Power and Efficiency for a Sodium Thermoelectric Heat Engine," Proc. 10th Intersociety Energy Conversion Engineering Conference, 2:231.

Ivanenok III, J.F, R.K. Sievers, T.K. Hunt, and G.A. Johnson (1993a), "Radioisotope AMTEC Power System Design for Sapcecraft Applications," Proc. 28th Intersociety Energy Conversion Engineering Conference, American Chemical Society, Washington, D.C., 1:665-660.

Ivanenok III, J.F, T.K. Hunt, and R.K. Sievers (1993b), "High Power Density AMTEC Systems," Proc. 28th Intersociety Energy Conversion Engineering Conference, American Chemical Society,

Washington, D.C.,1:861-865.

Kennard, E.H. (1938), *Kinetic Theory of Gases*, First Edition; McGraw-Hill: New York.

Sievers, R.K., T.K. Hunt, J.E. Pantolin, and D.A. Butkiewicz (1992), "Operation of Low Temperature AMTEC Cells," Proc. 27th Intersociety Energy Conversion Engineering Conference, 3:129.

Sievers, R.K., T.K. Hunt, J.F. Ivanenok III, and M.J. Schuller (1993), "Remote Condensing for High Efficiency AMTEC Cells," Proc. 28th Intersociety Energy Conversion Engineering Conference, American Chemical Society, Washington, D.C.,1:843-848.

Weber, N. (1974), "A Thermoelectric Device Based on Beta"-Alumina," *Energy Conversion*, 14:1-8.

White, F.M. (1986), *Fluid Mechanics*, Second Edition; McGraw-Hill: New York.

Williams, R.M., M.E. Loveland, B. Jeffries-Nakamura, M.L. Underwood, C.P. Bankston, H. Leduc, and J.T. Kummer (1990), "Kinetics and Transport in AMTEC Electrodes, I. The Interfacial Impedance Model," *J. Electrochemical Society*, 137: 1709-1716.